Stem Cell Reports
Article
ISSCR
OPEN ACCESS

Reprogramming epiblast stem cells into pre-implantation blastocyst cell-like cells

Kiichiro Tomoda,[1,2,3] Haiming Hu,[4] Yoshiki Sahara,[4,5,6] Hashimita Sanyal,[4] Minoru Takasato,[4,5] and Cody Kime[4,*]

[1]Gladstone Institutes, San Francisco, CA 94158, USA
[2]Center for iPS Cell Research and Application, Kyoto 606-8507, Japan
[3]Osaka Medical College, Osaka 569-8686, Japan
[4]RIKEN Center for Biosystems Dynamics Research, Kobe 650-0047, Japan
[5]Laboratory of Molecular Cell Biology and Development, Department of Animal Development and Physiology, Graduate School of Biostudies, Kyoto University, Kyoto 606-8501, Japan
[6]Department of Renal and Cardiovascular Research, New Drug Research Division, Otsuka Pharmaceutical Co. Ltd., Tokushima 771-0192, Japan
*Correspondence: cody.kime@riken.jp
https://doi.org/10.1016/j.stemcr.2021.03.016

SUMMARY

Recently, a new wave of synthetic embryo systems (SESs) has been established from cultured cells for efficient and ethical embryonic development research. We recently reported our epiblast stem cell (EPISC) reprogramming SES that generates numerous blastocyst (BC)-like hemispheres (BCLH) with pluripotent and extraembryonic cell features detected by microscopy. Here, we further explored the system over key time points with single-cell RNA-sequencing analysis. We found broad induction of the 2C-like reporter *MERVL* and RNA velocities diverging to three major cell populations with gene expression profiles resembling those of pluripotent epiblast, primitive endoderm, and trophectoderm. Enrichment of those three induced BC-like cell fates involved key gene-regulatory networks, zygotic genome activation-related genes, and specific RNA splicing, and many cells closely resembled *in silico* models. This analysis confirms the induction of extraembryonic cell populations during EPISC reprogramming. We anticipate that our unique BCLH SES and rich dataset may uncover new facets of cell potency, improve developmental biology, and advance biomedicine.

INTRODUCTION

Early embryonic development research was the basis for developmental biology and subsequent stem cell biology. In recent decades, much has been learned from mammalian embryology animal models that are not subject to the ethical considerations for human embryos (Hyun et al., 2020; Rossant and Tam, 2009, 2017). Early embryos were used to derive various pluripotent and multipotent stem cell lines with characteristics and chimera-integrating potential analogous to the assumed embryonic origin (Evans and Kaufman, 1981; Martin, 1981). However, the ability to form synthetic embryos from cultured cells had been elusive until recent advances enabled *in vitro* synthetic embryo systems (SESs) (Tomoda and Kime, 2021).

SESs are part of a newly emerging generation of models akin to organoids, but reflecting early embryology through "embryoids" that are far more convincing (Harrison et al., 2017; Kime et al, 2018, 2019; Rivron et al., 2018; Shahbazi and Zernicka-Goetz, 2018; Tomoda and Kime, 2021; Zheng et al., 2019). Several SESs exist, and some focus on modeling the blastocyst (BC) and its three layers: trophectoderm (TE), primitive endoderm (PE), and pluripotent pre-implantation epiblast (EPI). Some SESs utilize embryonic stem cell (ESC) and trophoblast stem cell (TSC) aggregations to model the pre-/post-implantation embryo *in vitro*. Other SESs, including those produced by our group, involve cell reprogramming or unique cell plasticity states that give rise to BC-like cysts from single cultures. Various approaches building on BC-like cyst formation *in vitro* continue to be developed and explored as each SES uniquely broadens embryology (Tomoda and Kime, 2021).

In a related field, reprogramming cells with exogenous factors (e.g., transcription factors, small molecules, cytokines, nutrients) pioneered new dimensions in cell biology by inducing donor cells to adopt desirable or unforeseen synthetic states (Davis et al., 1987; Kime et al, 2016, 2019; Takahashi et al., 2007; Woogeng et al., 2020). Indeed, analogs of early embryonic BC-lineage cells have been induced by many scientists (Benchetrit et al., 2019; Kubaczka et al., 2015; Parenti et al., 2016; Takahashi and Yamanaka, 2006). Our past epiblast stem cell (EPISC) reprogramming induced high-quality chimera-forming naive-like cells with X chromosome reactivation (Kime et al., 2016). We recently showed that the same reprogramming generated plates of BC-like hemispheres (BCLHs) with KRT8$^+$ (TROMA-I) TE-like cells surrounding the Xa/Xa EPI-like naive ESC region, which also had a PE-like GATA4$^+$/GATA6$^+$/PDGFRA$^+$ population at its inner face toward the putative blastocoel (Kime et al., 2018, 2019). However, detailed single-cell gene expression and regulation of the converting BCLH cells to resemble the three BC-lineage cells was previously unknown.

The BCLH SES can be easily set up and generates BCLHs efficiently from EPISC cultures. We established EPISCs with

the 2C-reporter *MERVL* and saw broad expression prior to BCLH cyst-like formation. We applied single-cell RNA sequencing (scRNA-seq) and saw that on day 5, three distinct regions of cells branched out with gene expression resembling the BC's TE, PE, and EPI lineages. The three regions each had RNA velocity toward day-7 cells that extended the regions and further enriched convincing cells of the postulated BC-cell identities. Furthermore, RNA splicing regulation and gene-regulatory networks implied that significant cell reprogramming had occurred with germ and zygotic genome activation (ZGA) signature genes. Here, we detail these observations and anticipate a welcome interest in the relatively poorly explored aspect of EPISC SES reprogramming into early embryonic cells.

RESULTS

Naive ESCs in 2iLIF may stabilize 2C/*MERVL*$^{+}$ reporter expression

For this study we required control naive ESCs to model early pluripotency. We therefore integrated *MERVL*::RFP reporters into B6N ESCs, which we cultured as previously reported (Kime et al., 2019). These cells are passaged with Accutase to single cells every few days on iMatrix511 in 6-well plates (see experimental procedures). Two distinct populations of ESCs stabilized within the same culture: one with the traditional dome-like morphology of naive ESCs with transient *MERVL*::RFP expression (Macfarlan et al., 2012) and the other with a unique larger cell morphology with sustained *MERVL*::RFP expression (Figure 1A). Our scRNA-seq analysis of the culture confirmed our suspicion of a "duality" because cells clustered into two distinct groups (Figure 1B) that we bisected at the origin of UMAP_1: the left cluster termed "ESC" and the right cluster with much more *MERVL*::RFP "2C-like" reporter expression we termed "ESC2CL" (Figures 1B and 1C). Although the cells were technically cultured and processed for scRNA-seq as one sample, the ESC2CL cells had much higher mean scRNA-seq features (ESC: 7,277; ESC2CL: 7,998; p value: 1.88711×10^{-119}) and counts (ESC: 53,285; ESC2CL: 69,568; p value: $2.576207 \times 10^{-108}$) shown by two-sample t test and violin plot (Figure S1A). These differences may come from ESC2CL cells being visibly larger or from harboring more mature transcripts accessible to the 3′ poly(A) priming of the scRNA-seq kit. When compared, both populations generally retained similar core pluripotency features (Figure 1D), and although differential gene markers could also be identified (Tables S1 and S2), there were few outstanding genes in each group's top 20 (Figure S1B). Because of their technical similarity in scRNA-seq data and our interest in 2C/*MERVL* regulation, we used both ESC and ESC2CL clusters throughout this study.

The BCLH SES induces 2C/*MERVL* reporter, XGFP, and three regions of blastocyst-like lineage cells

We previously generated (Kime et al., 2018, 2019) EPISCs with XGFP and *MERVL*::RFP reporters that are completely off when viewed by fluorescence microscopy (Figure 2A). We induced BCLH reprogramming with these cells and sampled them for scRNA-seq at day 5 and day 7, along with the starting EPISCs and the dual ESC/ESC2CL population, using a standard workflow including SkewC (Abugessaisa et al., 2020) to select high-quality cells for analysis (Figure S2A). On day 4 we rarely spotted XGFP expression while many cells showed *MERVL*::RFP activation that continued through day 5 and day 7 as XGFP became activated (Figure 2B). Activation of *MERVL* across full colonies was also visible with a rapidly degrading *MERVL*::D2nRFP reporter (Kime et al., 2018; Li et al., 1998) (Figure S2B).

We prepared our scRNA-seq samples with Seurat's SCTransform (Butler et al., 2018) and found a clear trend of three regions of cells on day 5 that clustered closely to similar expanded surrounding regions on day 7 (Figure 2C) across comparable ranges of features and counts with control cells (Figure S2C). In general, cells in the three regions often clustered together and the day-7 cells had more distinguished separation (Figure 2C). The EPISCs, the ESCs, and the ESC2CL cells clustered separately (Figure 2C). Surprisingly, many reprogramming cells in all regions had significant *MERVL*::RFP expression (Figures 2D and 2E), and mostly one specific region of day-7 cells expressed the XGFP reporter (Figure 2F) that may indicate naive pluripotent cells (Bao et al., 2009; Kime et al., 2016).

Checking gene expression revealed that common late BC-lineage cell markers were enriched and relatively focused in three separate regions characterized by Pluripotent/Epiblast-like, TE-like, and PE-like genes (Figures 2H–2J). The Epiblast-like region colocalized with the XGFP expression (Figure 2F) and was enriched for pluripotent genes (*Pou5f1*, *Zfp42*, *Tdgf1*, *Nr0b1*, *Klf2*) (Figure 2H). Importantly, XGFP was detected in the cells where *Klf2*, *Klf4*, and *Prdm14* were expressed (Figures 2F and 2H), consistent with the previously reported role of these genes in reactivating the inactive X chromosome (Gillich et al., 2012; Kime et al., 2016). In the TE-like region, we observed numerous important TE-establishing genes (*Ets2*, *Tfap2c*, *Gata2*, *Gata3*, *Elf4*) (Figure 2I) and remarkable expression of *Krt8* and *Krt18*, which were recently reported to organize extraembryonic fate determination in the compacting and polarizing embryo (Lim et al., 2020). We also found markers of more specialized TE-lineage cells (Hughes et al., 2013; Latos and Hemberger, 2016) enriched within the TE-like region (Figure S2D), suggesting some TE-lineage differentiation therein. Also, the smaller PE-like region had milder yet focused enrichment

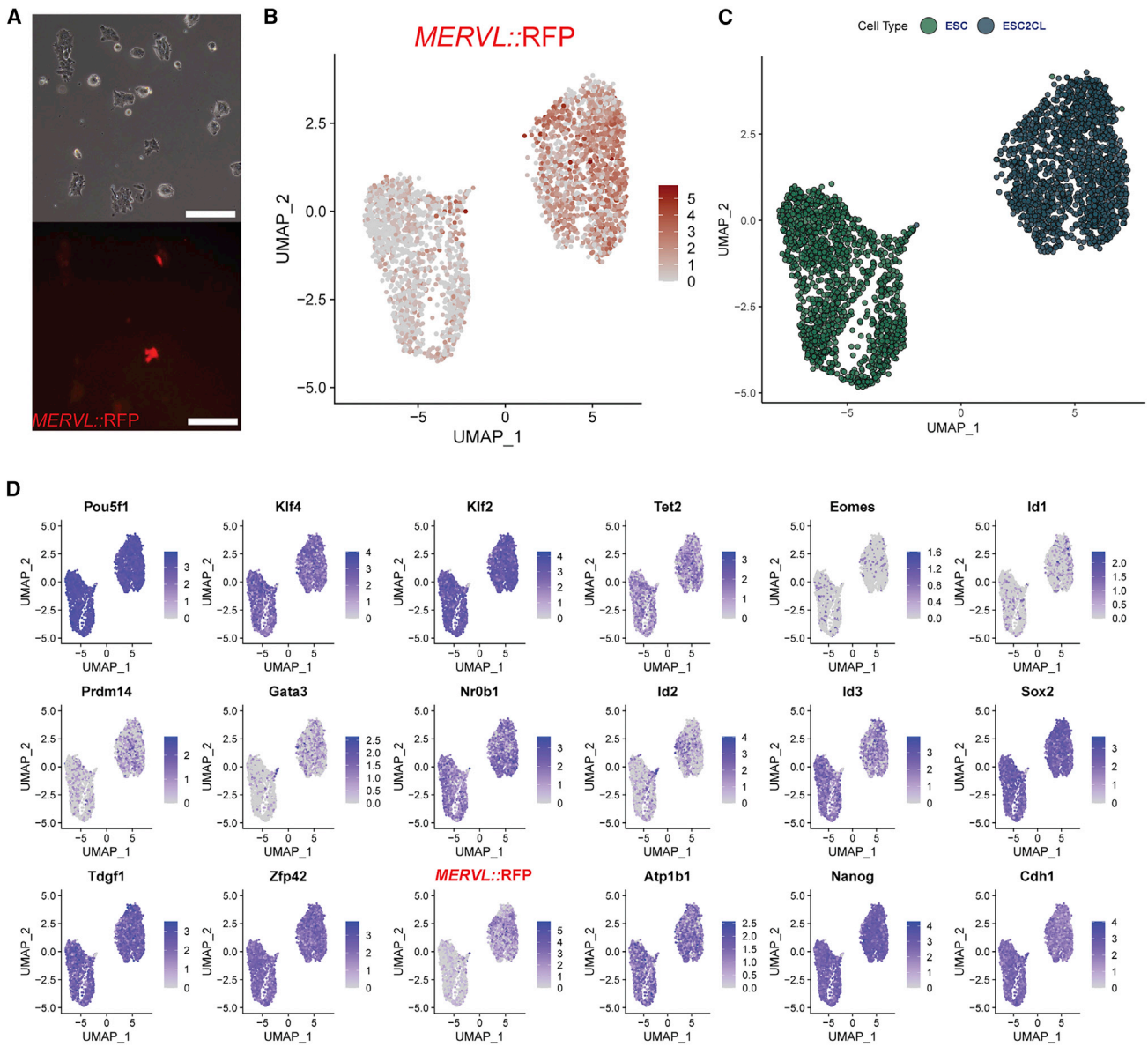

Figure 1. Mouse ESCs and *MERVL* reporter expression

(A) Duality of ESC culture in 2iLIF viewed with brightfield imaging (top) and *MERVL*::RFP expression (bottom). Scale bars, 200 μm.

(B) UMAP-based gene expression feature plot for transgenic *MERVL*::RFP.

(C) UMAP plot with labeled ESC and ESC2CL populations.

(D) UMAP-based gene expression feature plots for pluripotency genes.

for important PE genes (*Pdgfra*, *Gata4*, *Gata6*, *Fgfr1*, *Lifr*, *Lama1*) (Figure 2J).

The 2C-like *MERVL* reporter in ESCs has been used in several studies, yet its use in naive ESCs has been limited due to an unclear relationship to ZGA early embryonic-like plasticity. In our SESs we found utility with this reporter related to heightened cell plasticity (Kime et al., 2018, 2019). We therefore checked the expression of numerous recently reported ZGA-like regulators and ZGA signature genes derived from powerful screens (Alda-Catalinas et al., 2020). Many ZGA-like regulators were induced in reprogramming cells (Figure 2K), and ZGA signature genes were often highly expressed broadly or regionally in day-5 and day-7 reprogramming cells (Figure S2E), while many were not expressed in the stem cell controls including the ESC2CL cells (Figure S2E). As such, we hypothesize that ESCs may have a low threshold for *MERVL* reporter activation that reflects lesser 2C-like/ZGA gene

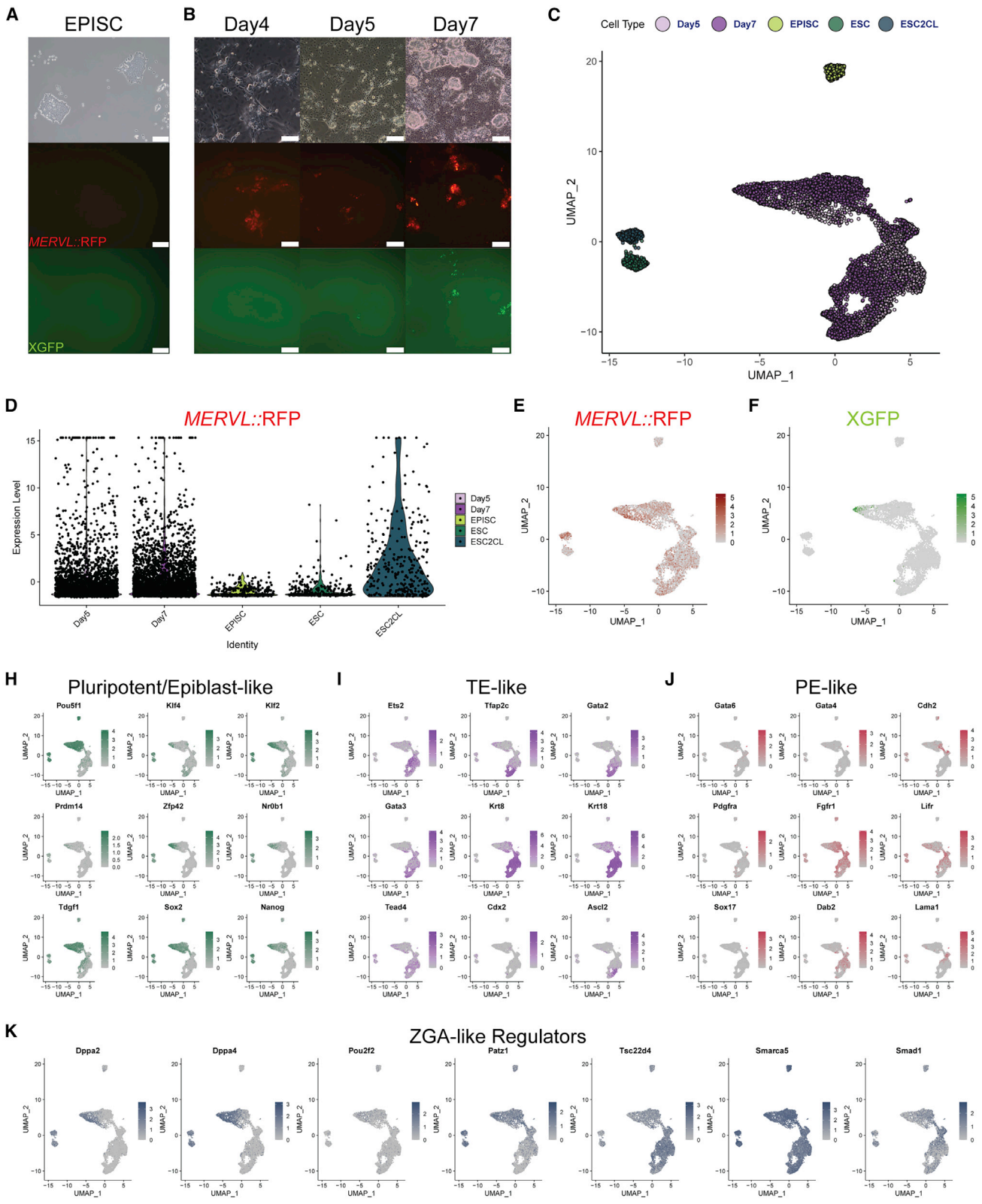

(legend on next page)

differences while *de novo MERVL* reporter activation in reprogramming cells might indicate a greater composition of ZGA-like genomic remodeling.

Three regions of blastocyst likeness enrich over time

To investigate the state of cells on day 5 and day 7, we employed RNA velocity with Velocyto (La Manno et al., 2018) to determine the "direction" of cell-state change and view RNA splice variation. The EPISC and the ESC/ESC2CL had RNA velocities pointing inward, demonstrating stable states (Figure 3A). As we anticipated, all three regions of the reprogramming cells displayed an obvious RNA velocity trend from day 5 toward day 7 and appeared to move away from each other (Figure 3A). Perhaps reflecting the PE formation of a BC, the ratio of cells driving into the PE-like region was fewer and distributed between the Epiblast-like and extraembryonic-like regions (Figures 2H–2J and 3A).

Discriminating unspliced (u) pre-mRNA versus spliced (s) mRNA ratios with scRNA-seq and Velocyto allows for a comprehensive understanding of important state-specific splice mechanisms beyond simple RNA detection. *Tdgf1* is an early BC inner cell mass (ICM) gene (Pfister et al., 2007) often detected in ESCs; however, *Tdgf1* was mostly unspliced in the ESC/ESC2CL clusters while strongly spliced and enriched in the Epiblast-like region of reprogramming cells (Figures 3A and 3B), where other gene expression seems to implicate a more ICM-like state. The germ programming genes *Prdm1* (*Blimp1*) and *Smc1b* were also splice-enriched in reprogramming cells (Figure S3A), supporting previous consideration of the importance of germ genes toward higher plasticity in our SES reprogramming (Kime et al., 2018, 2019). As seen in base expression (Figure 2K), the ZGA-like regulators *Dppa2*, *Dppa4*, *Tsc22d4*, *Smarca5*, and *Smad1* were induced across the reprogramming cells with splicing preference (Figure S3B), and the ESC2CL cells had spliced *Dppa2* more efficiently than the ESCs. Similar region-specific splice mechanism preference was found with TE and PE genes *Fgfr2* and *Lama1* (Figure 3B) for protein translation in putative cells. *Pard6b* and *Lifr* followed a similar trend while enriched in reprogramming cells' regions (Figure S3C). Taken together, the regulation of splice mechanisms and time-based BC-like cell region specification is apparent and related to pre-BC-stage regulators.

To investigate downstream gene regulation in reprogramming cells, we randomly downsampled the three regions to similar cell numbers after Seurat clusters 2:TE-like, 5:PE-like, and 4:Epiblast-like with day-specific labeling (Figure 3C). A heatmap of the top 100 global variable genes confirmed that each cluster had a unique pattern of expression (Figure 3D). We then performed SCENIC (Aibar et al., 2017) analysis of gene expression that infers upstream transcription factor DNA-binding activity to determine gene-regulatory network (regulons) enrichment that can robustly characterize cell identity. As expected, each region had distinct patterning that generally enriched from day 5 to day 7 (Figure S3D). The regulons were then binarized to simplify the interpretation of regulon activity. The pluripotent Epiblast-like population had largely lost primed pluripotency EPISC-specific regulons (e.g., *Pou3f1*) (Buecker et al., 2014) and reprogrammed with regulation remarkably similar to that of the ESC/ESC2CL with well-known naive pluripotency regulons (e.g. *Mybl2*, *Esrrb*, *Klf2*, *Klf4*), and shared broader pluripotency continuum regulons (e.g., *Sox2*, *Nanog*, *Pou5f1*) with EPISCs (Figure 3E) (Nichols and Smith, 2009; Weinberger et al., 2016). Not surprisingly, the ESC and ESC2CL populations had few differences at the regulatory level.

As anticipated, the PE-like and TE-like cells shared important extraembryonic regulons (e.g., *Klf6*, *Kdm5a*, *Creb3*, *Elf1*, *Elf4*) (Figure 3E) (Burton et al., 2013; Krendl et al., 2017; Rivron et al., 2018; Yang et al., 2013). Furthermore, the TE-like region had enriched significant TE-specific regulon activity (e.g., *Gata2*, *Gata3*, *Ascl2*, *Pparg*) (Figure 3E) including *Cdx2* regulon (Figure S3D) (Home et al., 2017; Krendl et al., 2017; Ralston et al., 2010). Also, the PE-like region had some enriched PE-specific regulon activity including *Gata6* and *Hnf1b* (Figure S3D) (Lo Nigro et al., 2017). Average gene expression for the same transcription factors of regulon analysis reflected a similar pattern

Figure 2. BCLH cell induction and regional gene expression

(A) EPISC culture with *MERVL*::RFP and XGFP reporters showing brightfield imaging (top) *MERVL*::RFP expression (middle), and XGFP expression (bottom). Scale bars, 200 μm.

(B) BCLH reprogramming from EPISC with *MERVL*::RFP and XGFP reporters imaged on day 4, day 5, and day 7, for brightfield (top), *MERVL*::RFP expression (middle), and XGFP expression (bottom). Scale bars, 100 μm (Day4) and 200 μm (Day5, Day7).

(C) UMAP plot clustering of EPISC, ESC, ESC2CL, day-5, and day-7 samples.

(D) Violin plot of transgenic *MERVL*::RFP reporter expression in EPISC, ESC, ESC2CL, day-5, and day-7 samples.

(E) UMAP-based gene expression feature plot for transgenic *MERVL*::RFP.

(F) UMAP-based gene expression feature plot for transgenic XGFP.

(H–J) UMAP-based gene expression feature plots for Pluripotent/Epiblast genes (H, green), TE genes (I, purple), and PE genes (J, burgundy) associated for BC-like regional likeness.

(K) UMAP-based gene expression feature plots for ZGA-like regulators.

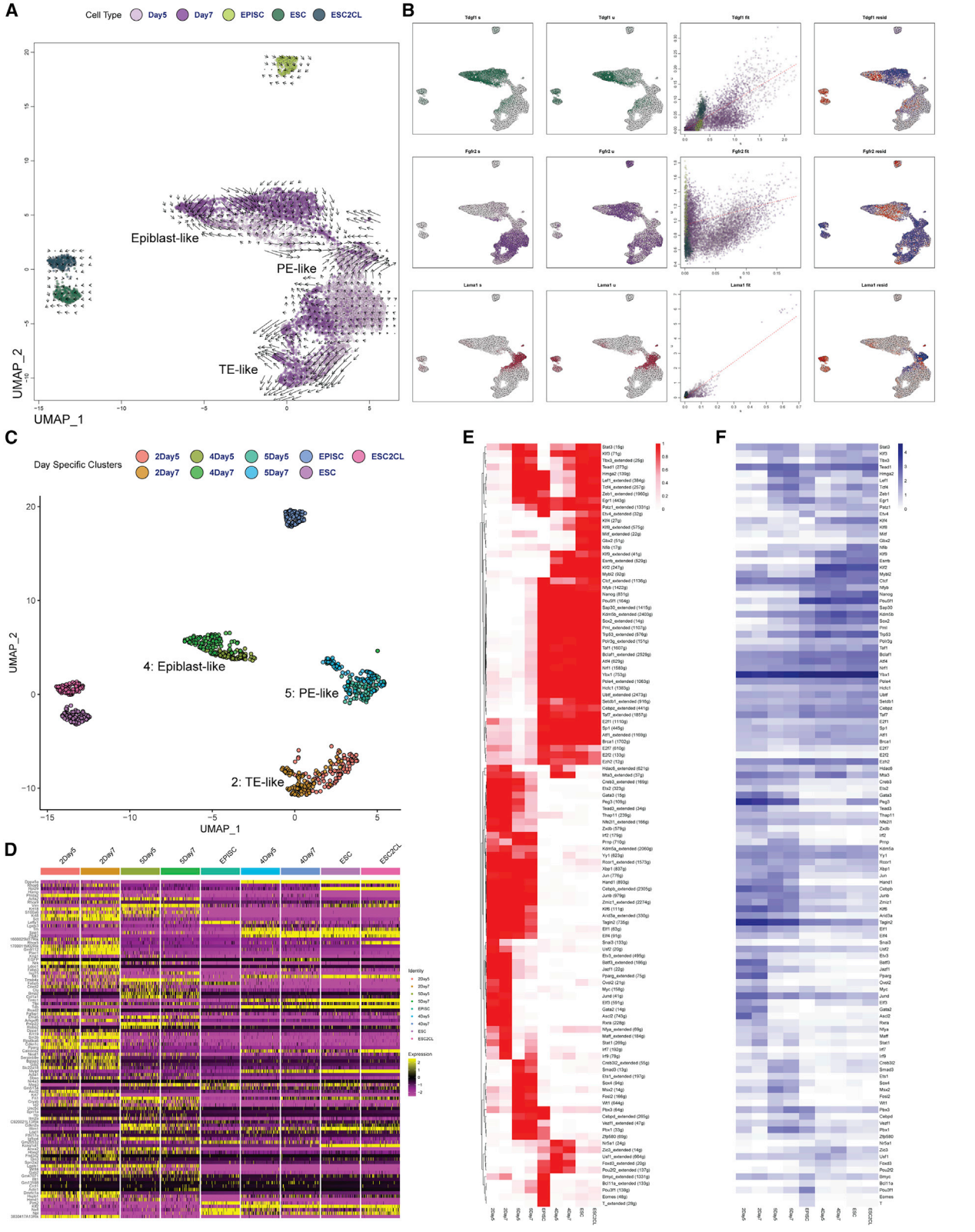

(legend on next page)

(Figure 3F), although far less specific, highlighting the value of gene-regulatory network analyses when comparing cells (Aibar et al., 2017; Woogeng et al., 2020).

The gene regulation and RNA splice differences raised uncanny distinction of the regions. We investigated numerous mouse RNA spliceosome genes (Kanehisa and Goto, 2000) and found some with discrete differences among the day-specific regions (Figure S4A). The *Mbnl* splice factors that repress naive pluripotency-specific splicing (Han et al., 2013) were only active in the TE-like and PE-like region cells (Figure S4A). Also, *Mbnl3*, a core trophoblast gene induced by *Gata3* and *Cdx2* (Ralston et al., 2010), was neatly expressed in the TE-like region. Interestingly, *Mbnl2* was one of the top 20 markers for the TE-like region among other TE genes (Figure S4B).

Taken together, the BCLH SES reprogramming cells formed three diverging regions over time with specific epigenetic splicing, expression, and downstream regulation that grossly reflected the three BC-cell lineages; such divergence over time may explain the controlled order and development of BCLHs observed in culture (Kime et al., 2019).

Some BCLH cells adopt the regulatory networks of established models

BCLH SES reprogramming induces many cells organized spatially like BCs (Kime et al., 2019). To better isolate and characterize the most BC-like cells *in silico*, we selected the induced cells that were most ICM/Epiblast-like (iEPI), TE-like (iTE), and PE-like (iPE) based on critical gene expression criteria (see experimental procedures). We also included comparable numbers of the ESCs/ESC2CL cells and starting EPISCs. For established TE and PE model cell data, we sourced a loom file (Posfai et al., 2021) that was built from established reports' scRNA-seq data. Using the 17,242 intersecting features of all samples, we then integrated with 5,000 anchors to correct for batch differences (see experimental procedures).

Seurat UMAP clustering from the integrated gene expression generally showed distinct populations based on type, although there was a general clustering of extraembryonic (iTE/TE/iPE/PE) samples (Figure 4A), similar to the TE/PE analysis in the model cell study (Posfai et al., 2021). Many TE and PE cells clustered together with iTE and iPE cells, likely from common extraembryonic expression. Excitingly, analysis with SCENIC showed distinct trends among 152 regulons that distinguished the putative similar cells (Figure 4B), demonstrated by the single-cell level total regulon activity plot (Figure S4C). SCENIC binarized regulon analysis revealed, again, the distinction between the pluripotency and extraembryonic cells with high similarity to established models (Figure S4D). Both SCENIC regulon plots (Figures 4B and S4D) had more clarity than average gene expression alone (Figure S4E), which highlighted the importance and power of gene-regulatory networks to determine a cell identity (Aibar et al., 2017). As expected, the iEPI cells were regulated alike to the ESCs/ESC2CL cells, having lost nearly all EPISC-specific regulons and acquiring regulons of naive pluripotency (Figure 4B) more clearly than the whole Epiblast-like cluster (Figure S3D). iPE/iTE samples had lost most EPISC-specific regulons that were also not found in the PE/TE cell models. In fact, the iPE/iTE and PE/TE model cells mostly had similar regulon enrichment profiles (Figure 4B) despite minor differences that appeared to come from a batch effect. Importantly, the iPE enriched key PE regulons (e.g., *Gata4*, *Gata6*, *Sox17*) and the iTE enriched many TE regulons (e.g., *Cdx2*, *Gata2*, *Klf6*).

We imported the regulon activity tables to the Seurat object and used FindMarkers to identify the top 10 regulon markers of the naive pluripotent, PE, and TE samples and plot their regulon activity (Figure S4F). Indeed, many top markers discovered were highly reported genes that define the correlating EPI/TE/PE cell states (e.g., *Klf2*, *Kfl4*, *Nanog*::*Cdx2*, *Ets2*, *Klf6*::*Sox7*, *Gata4*, *Gata6*) and were regulated relatively neatly among induced and model embryonic/extraembryonic populations (Figure S4F). In general, each of the three induced BC-like cell populations in BCLHs appeared to be regulated by the critical transcription factors of their putative equivalents.

Reclustering cells based on SCENIC regulon activity can provide clearer identity-based clustering (Aibar et al., 2017; Posfai et al., 2021). Upon doing so in t-distributed stochastic neighbor embedding (tSNE) map space, the

Figure 3. RNA velocity and gene regulation in the three BCLH regions

(A) UMAP-based RNA velocity plot for EPISC, ESC, ESC2CL, day-5, and day-7 samples with BC-like regions labeled based on regional gene expression (Figure 2).

(B) UMAP-based RNA splicing plots for spliced reads (s) and unspliced reads (u), with Cell Type coloring (A) and residual (resid) unspliced expression shown. RNAs detected are regionally labeled by color for pluripotency (green), TE (purple), and PE (burgundy).

(C) UMAP plot of downsampled day-specific cells and control cells for use in gene heatmap (D) and SCENIC regulon analysis (E and F; see also Figure S3D).

(D) Heatmap (DoHeatmap) plot of the top 100 variable features of all cells, ordered by day-specific regions of cells and control cells.

(E) SCENIC binarized regulons with heatmap (pheatmap) clustering and binarized regulon frequency (red scale) within the population.

(F) Heatmap (pheatmap) of the row-matched transcription factor average expression (log-transformed) for the regulons of (E).

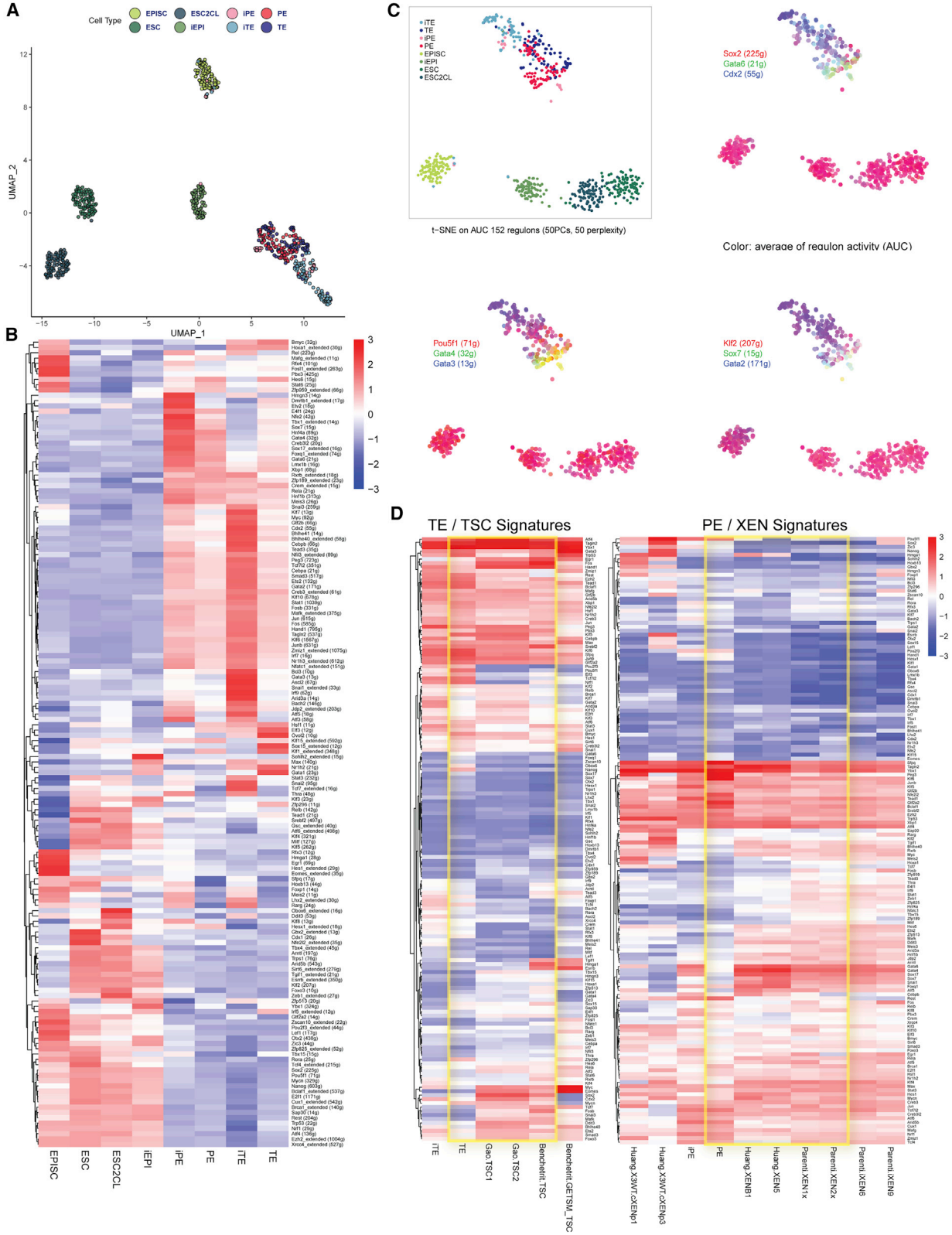

(legend on next page)

distinction of iTE/TE and iPE/PE marginally improved among better distinction between the pluripotent and extraembryonic states (Figure 4C). As seen with the regulon heatmaps (Figure 4B), the ESC and ESC2CL cell regulon activity caused those cells to nearly share the same tSNE space, strengthening the notion that these cells were more similar at the gene-regulatory level despite the stable *MERVL* reporter expression only in ESC2CL (Figures 4B and 4C). As expected, the iEPI cells now clustered closer to the ESCs/ESC2CL cells (Figure 4C). To view critical regulon activity in individual cells, we prepared three tSNE plots with BC-lineage-specific regulons on each plot that explained the regulatory activity responsible for the diverse cell types (Figure 4C, top right and bottom).

To learn more about the iTE and iPE identity reprogramming, we compared the sample gene expression with the model cells (TE and PE), with *in vitro* stem cell counterparts derived from natural BCs (TSC and XEN), and with *in vitro* reprogrammed cells (GETSM_TSC, cXEN, iXEN) from previously reported bulk RNA-seq data (Benchetrit et al., 2019; Gao et al., 2018; Huang et al., 2020; Parenti et al., 2016) (see experimental procedures). We based the gene list on the 152 regulon gene names that the SCENIC analysis learned while neatly separating our cells. Indeed, a core TE/TSC signature could be identified from the TE and TSCs, which was generally reflected in both reprogrammed iTE and GETSM_TSC. However, the iTE was closer to TE than to TSCs, possibly reflecting the differences between TE and TSCs, or batch effects (Figure 4D, left). Similarly, a core PE/XEN signature could be identified from the PE and XENs, which was well reflected in the iPE and iXEN samples and less clear for cXEN samples (Figure 4D, right).

Overall, the BCLH SES demonstrated remarkable cell reprogramming from primed pluripotent EPISCs that engaged sophisticated gene regulation and RNA splicing to produce regions and cell output (iEPI, iTE, and iPE) with the critical gene expression of pre-implantation embryo cells (TE/PE) and established cell lines (ESC/TSC/XEN).

DISCUSSION

Until now we had seen self-assembly and order that resembled BCs in the BCLH SES (Kime et al., 2018, 2019) that emerged in previous reprogramming works (Kime et al., 2016). In addition to confirming those observations, this study provides numerous insights into gene expression, RNA splicing regulation, and gene-regulatory networks that greatly strengthened our hypothesis that EPISCs can reprogram to represent BCs. The numerous ZGA signature and germ program related genes lead us to wonder how the cell reprogramming is engaged, although anticipated *Dux* and *Zscan4* expression was not detected at these time points (Hendrickson et al., 2017).

The BCLH SES is unique for its cell origin, defined culture conditions, and output. Given that the *MERVL* reporter activated early on, and day-5 cells neatly branched toward day 7, we anticipate that an earlier-time-point reprogramming precursor cell may exist. It will be important to dissect the reprogramming process with earlier time points and shorter intervals to fully understand how the initial reprogramming and lineage divergence occurs. Clues in unpublished aspects of this study continue to suggest germ program features as previously hypothesized (Kime et al., 2019). Discovery and optimization of a unique precursor, reprogrammed from EPISCs, may further advance our understanding of the distinctive properties of this SES. We anticipate that lineage tracing or cell selectivity based on the iEPI/iPE/iTE data may help discern key precursors and emerging populations. We would also like to include in scRNA-seq analysis early BC ICM cells and BC Epiblast-specific cells that we could not presently access.

The *MERVL* reporter has had significant utility in our SESs, and in the BCLH system it is more broadly induced than in the induced BC-like cysts (iBLCs) (Kime et al., 2019), where the defined conditions are altered in different phases. Conversely, BCLH SES cells proceeded more rapidly to form less organized BC-like hemispheres instead of puckering from the plate as floating self-organizing cysts. Since the *MERVL* reporter was highly active in all three regions of this study across day 5 and day 7, it provided some clues about unique 2C-like early embryonic programs that may be engaging the genome. Surprisingly, the ESC2CL cells in our base condition had sustained *MERVL*::RFP expression and had interesting differences from ESCs in gene expression despite overwhelming similarity at the gene-regulatory network level. We speculate that the *MERVL* reporter may have significant utility in our cell

Figure 4. Select BCLH SES cells reprogram meaningfully close to model cells

(A) UMAP-based plot for EPISC, ESC, ESC2CL, iEPI, iPE, iTE, PE, and TE samples.

(B) SCENIC total AUC regulon activity for EPISC, ESC, ESC2CL, iEPI, iPE, iTE, PE, and TE samples.

(C) Top-left panel: SCENIC tSNE plot based on AUC regulon activity. Top-right and bottom panels: average regulon activity at single-cell level in RGB color for pluripotency regulons (red), PE regulons (green), and TE regulons (blue) across the tSNE plot.

(D) Heatmap (pheatmap) of row-clustered TE/TSC signatures and PE/XEN signatures of reprogramming and model cells from this study and others (Benchetrit et al., 2019; Gao et al., 2018; Huang et al., 2020; Parenti et al., 2016; Posfai et al., 2021). Yellow outline surrounds the model cells (e.g., TE/TSC and PE/XEN), and cells outside the box are experimental (e.g., iTE/GETSM_TSC and cXEN/iPE/iXEN).

reprogramming that had numerous ZGA-related genes, yet wonder if our data here challenge the *MERVL* reporter's value in 2iLIF conditions.

Cell reprogramming

In general, the reprogramming cells lost their donor cell state and took on the programs of early BC-like cell lineages, which reflected prior observations in great detail. The XGFP$^+$ iEPI population was previously shown as readily potentiated for high contribution in chimeric embryos (Kime et al., 2016). Although TE-like and PE-like regions could be identified and harbored cells with convincing TE or PE properties, we wonder whether such cells could seed TSC or XEN cell cultures if transferred in selective conditions. In the BCLH SES, the TE-like region generally had infrequent *Cdx2* detection despite the specific enrichment of the *Cdx2* regulon, perhaps related to abundant keratin expression and TE-related transcription factor involvement. Interestingly, the TE can be specified independent of *Cdx2* (Wu et al., 2010). Although *Cdx2* is not required for BC formation (Meissner and Jaenisch, 2006), its role in implantation is important, and distinct CDX2$^+$ TE is roundly regarded (Strumpf et al., 2005). The PE-like region was less distinct and had significant overlap with the Epiblast-like and TE-like regions; perhaps the molecular distinction of the emerging iPE is as complicated as its natural ICM-to-extraembryonic transition at the late BC stage. Throughout this study we observed traces of gene expression suggesting that iPE and PE-like region cells shared a pluripotent-like origin with the iEPI population, reminiscent of the GATA4$^+$, GATA6$^+$, and PDGFRA$^+$ cells arising at the inner face of BCLH pluripotent cells (Kime et al., 2019). Consideration for PE cells has weighed heavily on various SESs (Tomoda and Kime, 2021), and we suspect that correct hypoblast formation will remain a hinge point for healthy embryoid development.

EXPERIMENTAL PROCEDURES

EPISC culture and BCLH reprogramming

EPISC culture and reprogramming was performed as described previously (Kime et al., 2016, 2019), and reprogramming included sodium pyruvate.

ESC culture and *MERVL* reporter integration

C57BL/6N (B6N) ESCs were converted from 3iLIF conditions and cultured in 2iLIF conditions with CTSFES basal medium as described previously (Kime et al., 2019) on iMatrix511-coated 6-well plates. Cells were integrated with and selected for *MERVL*::RFP reporters (mCherry and D2nmCherry) in piggyback vectors, the same as with EPISCs in our previous study (Kime et al., 2019). After several passages, the two different populations of ESC/ESC2CL cells became obvious and stabilized.

Microscopy

Brightfield and live-cell RFP and GFP fluorescence was imaged with an Olympus IX71 microscope.

scRNA-seq sampling and processing

Cells were dissociated and passed through cell screen cuvettes to isolate mostly healthy single cells that were prepared with 10X Genomics Chromium Single Cell 3′ Library & Gel Bead Kit V3.0. Sample libraries were finalized and sequenced on one Hiseq X lane (150 bp PE; Macrogen) for each. The Standard Cell Ranger protocol detected sample chemistry and produced "possorted" BAM files from which the subsequent Primary Analysis workflow in Figure S2A was performed to filter high-quality cells. For analyses shown in Figures 4 and S4, to match loom data counts for TE and PE control cells (Posfai et al., 2021) we prepared our data tables similarly with DESeq2 size factor normalization and log transformation. We integrated samples with intersecting features and Seurat CCA integration across 5,000 anchors. The iEPI, iTE, and iPE cell barcodes were selected from reprogramming cells with the following criteria:

iEPI: Zfp42 > 0.1 & Klf2 > 0.1 & EGFP > 0 & Prdm14 > 0.001
iTE: Cdx2 > 0 & Gata2 > 0
iPE: Gata6 > 0 & (Sox7 > 0 | Gata4 > 0 | Sox17 > 0)

Bulk external RNA-seq data processing

FPKM (fragments per kilobase per million mapped reads) tables from Gene Expression Omnibus accession numbers (GEO: GSE98124, GSM2805965, GSM2805966, GSE154398, GSM2054370, GSM2054371, GSM2054375, GSM2054376) were imported and log1p transformed. The first author's name of each selected external sample's related study was appended to the sample name for clarity (see Figure 4D). Genes of interest were reduced to the 152 gene names of the SCENIC regulons (Figure 4B). Our sample (iTE/TE/iPE/PE) relative count tables were added with log1p transformation. Each combined table was scaled together and generated in pheatmap with row-clustering and model cells at the center to clarify the signature patterns.

Data and code availability

All analysis code used in this study is available upon request. Raw and processed sequence data are accessible with accession number GEO: GSE166066.

SUPPLEMENTAL INFORMATION

Supplemental information can be found online at https://doi.org/10.1016/j.stemcr.2021.03.016.

AUTHOR CONTRIBUTIONS

Conceptualization, C.K.; Methodology, C.K. and K.T.; Experimentation, C.K., H.H., H.S., and Y.S.; Formal analysis, C.K. and K.T.; Investigation, C.K.; Resources, C.K., M.T., Y.S., and K.T.; Writing – original draft, C.K.; Writing – revision & editing, C.K. and K.T.; Visualization, C.K.; Project supervision, C.K.; Bioinformatics, C.K.; Project administration and funding, C.K.

CONFLICTS OF INTEREST

C.K. and K.T. have patents related to this technology and extended works.

ACKNOWLEDGMENTS

We are grateful for the support from RIKEN Center for Integrative Medical Sciences for specific training and research environment with support from Erik Arner, Piero Carninci, Imad Abugessaisa, Akira Hasegawa, and Teruaki Kitakura. We also thank Osamu Nishimura and the Shigehiro Kuraku lab at RIKEN for providing an HPC for Cell Ranger processing. We thank Eszter Posfai of Princeton University, and both Vincent Pasque and Adrian Janiszewski of Katholieke Universiteit Leuven for providing important control data and thoughtful discussions. We thank Ivo Woogeng Ngundu for specific support during this study. We also thank Francoise Chanut for copy-editing the manuscript.

This study was primarily funded by the RIKEN Center for Biosystems Dynamics Research Organoid Project. K.T. was supported by the iPS Cell Research Fund from Center for iPS Cell Research and Application, Kyoto University, Core Center for iPS Cell Research (19bm0104001h0007), Research Center Network for Realization of Regenerative Medicine from AMED (Japan Agency for Medical Research and Development), and the L.K. Whittier Foundation.

Received: September 30, 2020
Revised: March 16, 2021
Accepted: March 16, 2021
Published: May 11, 2021

REFERENCES

Abugessaisa, I., Noguchi, S., Cardon, M., Hasegawa, A., Watanabe, K., Takahashi, M., Suzuki, H., Katayama, S., Kere, J., and Kasukawa, T. (2020). Quality assessment of single-cell RNA sequencing data by coverage skewness analysis. BioRxiv https://doi.org/10.1101/2019.12.31.890269.

Aibar, S., González-Blas, C.B., Moerman, T., Huynh-Thu, V.A., Imrichova, H., Hulselmans, G., Rambow, F., Marine, J.-C., Geurts, P., Aerts, J., et al. (2017). SCENIC: single-cell regulatory network inference and clustering. Nat. Methods *14*, 1083–1086.

Alda-Catalinas, C., Bredikhin, D., Hernando-Herraez, I., Santos, F., Kubinyecz, O., Eckersley-Maslin, M.A., Stegle, O., and Reik, W. (2020). A single-cell transcriptomics CRISPR-activation screen identifies epigenetic regulators of the zygotic genome activation program. Cell Syst. *11*, 25–41.e9.

Bao, S., Tang, F., Li, X., Hayashi, K., Gillich, A., Lao, K., and Surani, M.A. (2009). Epigenetic reversion of post-implantation epiblast to pluripotent embryonic stem cells. Nature *461*, 1292–1295.

Benchetrit, H., Jaber, M., Zayat, V., Sebban, S., Pushett, A., Makedonski, K., Zakheim, Z., Radwan, A., Maoz, N., Lasry, R., et al. (2019). Direct induction of the three pre-implantation blastocyst cell types from fibroblasts. Cell Stem Cell *24*, 983–994.e7.

Buecker, C., Srinivasan, R., Wu, Z., Calo, E., Acampora, D., Faial, T., Simeone, A., Tan, M., Swigut, T., and Wysocka, J. (2014). Reorganization of enhancer patterns in transition from naive to primed pluripotency. Cell Stem Cell *14*, 838–853.

Burton, A., Muller, J., Tu, S., Padilla-Longoria, P., Guccione, E., and Torres-Padilla, M.-E. (2013). Single-cell profiling of epigenetic modifiers identifies PRDM14 as an inducer of cell fate in the mammalian embryo. Cell Rep. *5*, 687–701.

Butler, A., Hoffman, P., Smibert, P., Papalexi, E., and Satija, R. (2018). Integrating single-cell transcriptomic data across different conditions, technologies, and species. Nat. Biotechnol. *36*, 411–420.

Davis, R.L., Weintraub, H., and Lassar, A.B. (1987). Expression of a single transfected cDNA converts fibroblasts to myoblasts. Cell *51*, 987–1000.

Evans, M.J., and Kaufman, M.H. (1981). Establishment in culture of pluripotential cells from mouse embryos. Nature *292*, 154–156.

Gao, H., Gao, R., Zhang, L., Xiu, W., Zang, R., Wang, H., Zhang, Y., Chen, J., Gao, Y., and Gao, S. (2018). Esrrb plays important roles in maintaining self-renewal of trophoblast stem cells (TSCs) and reprogramming somatic cells to induced TSCs. J. Mol. Cell Biol. *11*, 463–473.

Gillich, A., Bao, S., Grabole, N., Hayashi, K., Trotter, M.W.B., Pasque, V., Magnúsdóttir, E., and Surani, M.A. (2012). Epiblast stem cell-based system reveals reprogramming synergy of germline factors. Cell Stem Cell *10*, 425–439.

Han, H., Irimia, M., Ross, P.J., Sung, H.-K., Alipanahi, B., David, L., Golipour, A., Gabut, M., Michael, I.P., Nachman, E.N., et al. (2013). MBNL proteins repress ES-cell-specific alternative splicing and reprogramming. Nature *498*, 241–245.

Harrison, S.E., Sozen, B., Christodoulou, N., Kyprianou, C., and Zernicka-Goetz, M. (2017). Assembly of embryonic and extraembryonic stem cells to mimic embryogenesis in vitro. Science *356*, eaal1810.

Hendrickson, P.G., Doráis, J.A., Grow, E.J., Whiddon, J.L., Lim, J.-W., Wike, C.L., Weaver, B.D., Pflueger, C., Emery, B.R., Wilcox, A.L., et al. (2017). Conserved roles of mouse DUX and human DUX4 in activating cleavage-stage genes and MERVL/HERVL retrotransposons. Nat. Genet. *49*, 925–934.

Home, P., Kumar, R.P., Ganguly, A., Saha, B., Milano-Foster, J., Bhattacharya, B., Ray, S., Gunewardena, S., Paul, A., Camper, S.A., et al. (2017). Genetic redundancy of GATA factors in the extraembryonic trophoblast lineage ensures the progression of preimplantation and postimplantation mammalian development. Development *144*, 876–888.

Huang, X., Bashkenova, N., Yang, J., Li, D., and Wang, J. (2020). ZFP281 recruits polycomb repressive complex 2 to restrict extraembryonic endoderm potential in safeguarding embryonic stem cell pluripotency. Protein Cell *12*, 213–219.

Hughes, M., Natale, B.V., Simmons, D.G., and Natale, D.R.C. (2013). Ly6e expression is restricted to syncytiotrophoblast cells of the mouse placenta. Placenta *34*, 831–835.

Hyun, I., Munsie, M., Pera, M.F., Rivron, N.C., and Rossant, J. (2020). Toward guidelines for research on human embryo models formed from stem cells. Stem Cell Reports *14*, 169–174.

Kanehisa, M., and Goto, S. (2000). KEGG: Kyoto Encyclopedia of Genes and Genomes. Nucleic Acids Res. *28*, 27–30.

Kime, C., Sakaki-Yumoto, M., Goodrich, L., Hayashi, Y., Sami, S., Derynck, R., Asahi, M., Panning, B., Yamanaka, S., and Tomoda, K. (2016). Autotaxin-mediated lipid signaling intersects with LIF and BMP signaling to promote the naive pluripotency transcription factor program. Proc. Natl. Acad. Sci. U S A *113*, 12478–12483.

Kime, C., Kiyonari, H., Ohtsuka, S., Kohbayashi, E., Asahi, M., Yamanaka, S., Takahashi, M., and Tomoda, K. (2018). Implantation-competent blastocyst-like structures from mouse pluripotent stem cells. BioRxiv https://doi.org/10.1101/309542.

Kime, C., Kiyonari, H., Ohtsuka, S., Kohbayashi, E., Asahi, M., Yamanaka, S., Takahashi, M., and Tomoda, K. (2019). Induced 2C expression and implantation-competent blastocyst-like cysts from primed pluripotent stem cells. Stem Cell Reports *13*, 485–498.

Krendl, C., Shaposhnikov, D., Rishko, V., Ori, C., Ziegenhain, C., Sass, S., Simon, L., Müller, N.S., Straub, T., Brooks, K.E., et al. (2017). GATA2/3-TFAP2A/C transcription factor network couples human pluripotent stem cell differentiation to trophectoderm with repression of pluripotency. Proc. Natl. Acad. Sci. U S A *114*, E9579–E9588.

Kubaczka, C., Senner, C.E., Cierlitza, M., Araúzo-Bravo, M.J., Kuckenberg, P., Peitz, M., Hemberger, M., and Schorle, H. (2015). Direct induction of trophoblast stem cells from murine fibroblasts. Cell Stem Cell *17*, 557–568.

La Manno, G., Soldatov, R., Zeisel, A., Braun, E., Hochgerner, H., Petukhov, V., Lidschreiber, K., Kastriti, M.E., Lönnerberg, P., Furlan, A., et al. (2018). RNA velocity of single cells. Nature *560*, 494–498.

Latos, P.A., and Hemberger, M. (2016). From the stem of the placental tree: trophoblast stem cells and their progeny. Development *143*, 3650–3660.

Li, X., Zhao, X., Fang, Y., Jiang, X., Duong, T., Fan, C., Huang, C.-C., and Kain, S.R. (1998). Generation of destabilized green fluorescent protein as a transcription reporter. J. Biol. Chem. *273*, 34970–34975.

Lim, H.Y.G., Alvarez, Y.D., Gasnier, M., Wang, Y., Tetlak, P., Bissiere, S., Wang, H., Biro, M., and Plachta, N. (2020). Keratins are asymmetrically inherited fate determinants in the mammalian embryo. Nature *585*, 404–409.

Lo Nigro, A., de Jaime-Soguero, A., Khoueiry, R., Cho, D.S., Ferlazzo, G.M., Perini, I., Abon Escalona, V., Aranguren, X.L., Chuva de Sousa Lopes, S.M., Koh, K.P., et al. (2017). PDGFRα^{+} cells in embryonic stem cell cultures represent the in vitro equivalent of the pre-implantation primitive endoderm precursors. Stem Cell Reports *8*, 318–333.

Macfarlan, T.S., Gifford, W.D., Driscoll, S., Lettieri, K., Rowe, H.M., Bonanomi, D., Firth, A., Singer, O., Trono, D., and Pfaff, S.L. (2012). Embryonic stem cell potency fluctuates with endogenous retrovirus activity. Nature *487*, 57–63.

Martin, G.R. (1981). Isolation of a pluripotent cell line from early mouse embryos cultured in medium conditioned by teratocarcinoma stem cells. Proc. Natl. Acad. Sci. U S A *78*, 7634–7638.

Meissner, A., and Jaenisch, R. (2006). Generation of nuclear transfer-derived pluripotent ES cells from cloned Cdx2-deficient blastocysts. Nature *439*, 212–215.

Nichols, J., and Smith, A. (2009). Naive and primed pluripotent states. Cell Stem Cell *4*, 487–492.

Parenti, A., Halbisen, M.A., Wang, K., Latham, K., and Ralston, A. (2016). OSKM induce extraembryonic endoderm stem cells in parallel to induced pluripotent stem cells. Stem Cell Reports *6*, 447–455.

Pfister, S., Steiner, K.A., and Tam, P.P.L. (2007). Gene expression pattern and progression of embryogenesis in the immediate post-implantation period of mouse development. Gene Expr. Patterns *7*, 558–573.

Posfai, E., Schell, J.P., Janiszewski, A., Rovic, I., Murray, A., Bradshaw, B., Yamakawa, T., Pardon, T., El Bakkali, M., Talon, I., et al. (2021). Evaluating totipotency using criteria of increasing stringency. Nat. Cell Biol. *23*, 49–60.

Ralston, A., Cox, B.J., Nishioka, N., Sasaki, H., Chea, E., Rugg-Gunn, P., Guo, G., Robson, P., Draper, J.S., and Rossant, J. (2010). Gata3 regulates trophoblast development downstream of Tead4 and in parallel to Cdx2. Development *137*, 395–403.

Rivron, N.C., Frias-Aldeguer, J., Vrij, E.J., Boisset, J.-C., Korving, J., Vivié, J., Truckenmüller, R.K., van Oudenaarden, A., van Blitterswijk, C.A., and Geijsen, N. (2018). Blastocyst-like structures generated solely from stem cells. Nature *557*, 106–111.

Rossant, J., and Tam, P.P. (2009). Blastocyst lineage formation, early embryonic asymmetries and axis patterning in the mouse. Development *136*, 701–713.

Rossant, J., and Tam, P.P.L. (2017). New insights into early human development: lessons for stem cell derivation and differentiation. Cell Stem Cell *20*, 18–28.

Shahbazi, M.N., and Zernicka-Goetz, M. (2018). Deconstructing and reconstructing the mouse and human early embryo. Nat. Cell Biol. *20*, 878.

Strumpf, D., Mao, C.-A., Yamanaka, Y., Ralston, A., Chawengsaksophak, K., Beck, F., and Rossant, J. (2005). Cdx2 is required for correct cell fate specification and differentiation of trophectoderm in the mouse blastocyst. Development *132*, 2093–2102.

Takahashi, K., and Yamanaka, S. (2006). Induction of pluripotent stem cells from mouse embryonic and adult fibroblast cultures by defined factors. Cell *126*, 663–676.

Takahashi, K., Tanabe, K., Ohnuki, M., Narita, M., Ichisaka, T., Tomoda, K., and Yamanaka, S. (2007). Induction of pluripotent stem cells from adult human fibroblasts by defined factors. Cell *131*, 861–872.

Tomoda, K., and Kime, C. (2021). Synthetic embryology: early mammalian embryo modeling systems from cell cultures. Dev. Growth Differ. https://doi.org/10.1111/dgd.12713.

Weinberger, L., Ayyash, M., Novershtern, N., and Hanna, J.H. (2016). Dynamic stem cell states: naive to primed pluripotency in rodents and humans. Nat. Rev. Mol. Cell Biol. *17*, 155–169.

Woogeng, I.N., Abugessaisa, I., Tachibana, A., Sahara, Y., Hon, C.-C., Hasegawa, A., Kaczkowski, B., Sakai, N., Nishida, M., Hu, H., et al. (2020). Inducing human retinal pigment epithelium-like cells

from somatic tissue. BioRxiv https://doi.org/10.1101/2020.07.27.215103.

Wu, G., Gentile, L., Fuchikami, T., Sutter, J., Psathaki, K., Esteves, T.C., Araúzo-Bravo, M.J., Ortmeier, C., Verberk, G., Abe, K., et al. (2010). Initiation of trophectoderm lineage specification in mouse embryos is independent of Cdx2. Development *137*, 4159–4169.

Yang, Y., JIN, Y., MARTYN, A.C., LIN, P., SONG, Y., CHEN, F., HU, L., CUI, C., LI, X., LI, Q., et al. (2013). Expression pattern implicates a potential role for luman recruitment factor in the process of implantation in uteri and development of preimplantation embryos in mice. J. Reprod. Dev. *59*, 245–251.

Zheng, Y., Xue, X., Shao, Y., Wang, S., Esfahani, S.N., Li, Z., Muncie, J.M., Lakins, J.N., Weaver, V.M., Gumucio, D.L., et al. (2019). Controlled modelling of human epiblast and amnion development using stem cells. Nature *573*, 421–425.